Arch Appl Mech (2012) 82:229–242
DOI 10.1007/s00419-011-0552-x

ORIGINAL

Yahya Bayat · Mahdi Ghannad · Hamid Torabi

Analytical and numerical analysis for the FGM thick sphere under combined pressure and temperature loading

Received: 27 December 2010 / Accepted: 8 May 2011 / Published online: 26 May 2011

Abstract Thermo-mechanical analysis of functionally graded hollow sphere subjected to mechanical loads and one-dimensional steady-state thermal stresses is carried out in this study. The material properties are assumed to vary non-linearly in the radial direction, and the Poisson's ratio is assumed constant. The temperature distribution is assumed to be a function of radius, with general thermal and mechanical boundary conditions on the inside and outside surfaces of the sphere. In the analysis presented here, the effect of non-homogeneity in FGM thick sphere was implemented by choosing a dimensionless parameter, named $\beta_i (i = 1, \ldots, 3)$, which could be assigned an arbitrary value affecting the stresses in the sphere. It is observed that the solution process for $\beta_i (i = 3) = -1$ are different from those obtained for other values of $\beta_i (i = 1, \ldots, 3)$. Cases of pressure, temperature, and combined loadings were considered separately. It is concluded that by changing the value of $\beta_i (i = 1 \ldots 3)$, the properties of FGM can be so modified that the lowest stress levels are reached. The present results agree well with existing results. Using FEM simulations, the analytical findings for FGM spheres under the influence of internal pressure and temperature gradient were compared to finite element results.

Keywords FGM · Analytical · FEM · Hallow sphere · Dimensionless ·

1 Introduction

Functionally graded materials (FGMs) are being increasingly considered in various applications in the recent years. These materials have received considerable attention in many engineering applications since they were first reported in 1984 in Japan [1,2]. Actually, FGMs are mixtures of two or more different materials. Volume fraction of each material varies continuously along certain direction(s). The gradual change in material properties can be tailored to meet the requirements of different applications and working environments. The FGMs were initially designed as thermal barrier materials for aerospace structures.

Compared with the fiber-reinforced or laminated composite materials, FGMs are more preferable in many thermal–mechanical applications. It is because continuous change in the microstructure of FGMs may not be subjected to a mismatch of mechanical properties across the interface as a reinforced or laminated material does. As a result, these materials are able to withstand high-temperature gradients without structural failures. This feature is vital, especially in space and aeronautical applications. The aims of researchers are to understand the effect of composition on stresses and to design the optimum FGM hollow circular cylinder and sphere.

During the past years, many researchers have studied the characteristic behavior of FGMs under different loading conditions. Tanigawa [3] presented an extensive review that covered a wide range of topics from

Y. Bayat (✉) · M. Ghannad
Department of Mechanical Engineering, Shahrood University of Technology, Daneshgah Blvd., Shahrood, Iran
E-mail: torabi.mech87@gmail.com

H. Torabi
Islamic Azad University, Mashhad Branch, Young Researchers Club, Mashhad, Iran

thermoelastic to thermo-inelastic problems. He compiled a comprehensive list of papers on the analytical models of thermoelastic behavior of FGMs. Obata and Noda [4] studied the steady-state thermal stresses in FGM hollow cylinders and spheres to understand the effect of the volumetric ratio of constituents and porosity on thermal stresses. The unsteady-state thermal stress of FGM circular hollow cylinders based on the multilayered method was presented by Kim and Noda [5] by using Green function method. A work was also published by Horgan and Chan [6] where it was noted that increasing the positive exponent of the radial coordinate provided a stress shielding effect, whereas decreasing it created stress amplification. Nayebi and Abdi [7] developed a numerical program to investigate the steady-state behavior of thick-walled spherical and cylindrical pressure vessels subjected to cyclic pressure and/or temperature using linear kinematic hardening in the plastic condition and a Norton power law in the creep condition. Geometric non-linearity and effect of coupling item for different thermal loading conditions were considered in the works of Reddy et al. [8–13]. They carried out theoretical as well as finite element analyses of the thermo-mechanical behavior of FGM cylinders, plates, and shells.

Much research has been conducted on isotropic or laminated composite plates and shells. However, it seems that very little has been done on FGM thick vessels. Analytical solutions have been done by Johnson and Mellor [14] for thick cylindrical vessels under pressure and temperature loading. Applying the Frobenius series method, Zimmerman and Lutz [15] found a way round the problem of the uniform heating of FG circular cylinder. They derived the exact solution for the problem of radially heated cylinder whose modulus of elasticity and thermal expansion coefficient vary linearly with radius. Exact solutions for stresses in FG pressure vessels were given by Tutuncu and Ozturk [16]. They obtained the closed-form solutions for stresses and displacements in FG cylindrical and spherical vessels under internal pressure. Another general analysis of one-dimensional steady-state thermal stresses in a hollow thick cylinder made of FGM was obtained by Eslami et al. [17]. They used a direct method to solve the heat conduction and Navier equations. Furthermore, the temperature distribution was assumed to be a function of radius. In a similar work, Eslami et al. [18] investigated the thermal and mechanical stresses in a FGM sphere using the same method as in [17]. In addition, Poultangari et al. [19] studied the thermal and mechanical stresses in a FGM sphere under non-axisymmetric thermo-mechanical loads. An alternate analytical method to carry out the elastic analysis of thick-walled spherical pressure vessels subjected to internal pressure was presented by You et al. [20]. They considered two kinds of pressure vessel: one consists of two homogeneous layers near the inner and outer surfaces of the vessel and one functionally graded layer in the middle and another only consists of the FGM.

Pan and Roy [21] derived exact solutions for multilayered FGM cylinders under static deformation. They obtained these solutions by making use of the method of separation of variables and expressed it in terms of the summation of the Fourier series in the circumferential direction. Jabbari et al. [22] making use of the generalized Bessel function and Fourier series solved the temperature and Navier equations analytically and offered a general theoretical analysis of three-dimensional mechanical and thermal stresses for a short hollow cylinder made of functionally graded material. In a study carried out by You et al. [23], the deformations and stresses in thick-walled cylindrical vessels made of FGMs were obtained. Such vessels have a varying Young's modulus and thermal expansion coefficient and are subjected to internal pressure and uniform temperature change. Given the assumption that the material is isotropic with constant Poisson's ratio and exponentially varying modulus of elasticity through the thickness, thermal and mechanical stresses in a FGM sphere for exponentially varying material properties were obtained by Eslami et al. [24]. Tutuncu [25] obtained power series solutions for stresses and displacements in FG cylindrical vessels subjected to internal pressure alone. In a recent study by Chen and Lin [26], assuming that the property of FGMs is in exponential function form, they conducted the elastic analyses for both a thick cylinder and a spherical pressure vessel which was made of functionally graded materials. In this paper, thermo-mechanical properties of functionally graded materials were assumed to be temperature independent and vary continuously in the radial direction of the cylinder. Abrinia et al. [27] presented a new analysis for the FGM thick cylinders under combined pressure and temperature Loadings. They obtained the distribution of stresses in radial and circumferential directions for FGM cylinders under the influence of internal pressure and temperature gradient. Zamani Nejad and Rahimi [28] investigated the thermal and mechanical stresses under generalized plane strain and plane stress assumptions, respectively. Concerning the stress analysis of cylindrical and spherical structural elements, Tutuncu and Temel [29] presented a novel approach to stress analysis of pressurized FGM cylinders, disks, and spheres. In this work, axisymmetric displacements and stresses in functionally graded hollow cylinders, disks, and spheres subjected to uniform internal pressure were determined using plane elasticity theory and complementary functions method.

In this paper, a thick hollow sphere made of FGM under one-dimensional steady-state temperature distribution with general types of boundary conditions (thermal and mechanical) was studied. The thermal and mechanical properties of the sphere were expressed as power law functions of the radial direction. The heat conduction and Navier equations were solved to obtain the analytical solution of the problem. Finally, the analytical results for a FG hollow sphere under spherically symmetric thermo-mechanical loadings were compared with finite element results. This analysis uses the basic equation suggested by references [14,18] and extends them to include the effect of temperature as well. The arbitrary values used in this study for the inhomogeneity constant β do not necessarily represent a certain material.

2 Theoretical formulation and equilibrium equations

Consider a thick hollow sphere made of FGM, with the internal radius "a" and external radius "b" and "r", which is normalized as $r = \frac{R}{a}$ where "R" having a value between "a" and "b". For the following analysis, a spherical coordinate system (R, ϕ, θ) is adopted with the origin at the center of the sphere. The geometry of the sphere in relation with the coordinate axes is shown in Fig. 1. Then, in order to account for the changing material properties along the radius, a power law relationship [18] is used as follows

$$E(r) = E_i r^{\beta_1}, \quad \alpha(r) = \alpha_i r^{\beta_2}, \quad \lambda(r) = \lambda_i r^{\beta_3}, \tag{1a, b, c}$$

where β_1, β_2, and β_3 are the power law indices of the material. Substituting $r = 1$ in above equation could draw that E_i, α_i, and λ_i are the modulus of elasticity, the coefficient of thermal expansion, and thermal conductivity coefficient of inner surface, respectively.

Note that the value of Poisson's ratio has been taken as constant because although the material is not homogenous but considering that all materials almost have a constant Poisson's ratio value in the elastic range, this is a reasonable assumption. Now the formulation begins with the expressions for the strain and stress distributions through the thickness of the sphere using the equilibrium equation as follows

$$\frac{\mathrm{d}\sigma_r}{\mathrm{d}r} + \frac{2}{r}(\sigma_r - \sigma_\phi) = 0, \tag{2}$$

where σ_r and σ_ϕ are the radial and circumferential stress components, respectively. For spherically symmetric problem, we have $u_\theta = u_\phi = 0$ and $u_r = u_r(r)$, where $u_i (i = r, \phi, \theta)$ are the components of displacement respectively. Then, the strain–displacement relations are simplified as

$$\varepsilon_r = \frac{\mathrm{d}u_r}{\mathrm{d}r}, \quad \varepsilon_\phi = \frac{u_r}{r}. \tag{3a, b}$$

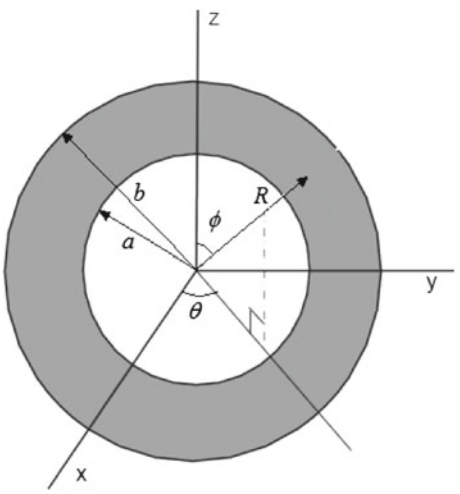

Fig. 1 Cross-section of a cylindrical pressure vessel with internal radius "a" and external radius "b"

It could be easily shown that the stresses in the radial and circumferential directions are given by

$$\sigma_r = \frac{E_i r^{\beta_1}}{(1+\nu)(1-2\nu)}\left[(1-\nu)\varepsilon_r + 2\nu\varepsilon_\phi - (1+\nu)\alpha_i r^{\beta_2} T(r)\right], \tag{4a}$$

$$\sigma_\phi = \sigma_\theta = \frac{E_i r^{\beta_1}}{(1+\nu)(1-2\nu)}\left[\nu\varepsilon_r + \varepsilon_\phi - (1+\nu)\alpha_i r^{\beta_2} T(r)\right], \tag{4b}$$

where $T(r)$ is the temperature distribution determined from the heat conduction equation. The substitution of Eqs. (4) and (3a, b) into Eq. (2) produces the Navier equation

$$r^2 u_r'' + A r u_r' + B u_r = \frac{1+\nu}{1-\nu}\alpha_i r^{\beta_2}\left\{r(\beta_1+\beta_2)T(r) + r^2 T'(r)\right\}, \tag{5}$$

where

$$A = 2 + \beta_1, \quad B = \frac{2\left[\nu(\beta_1+1)-1\right]}{1-\nu}. \tag{6a, b}$$

and $(')$ denotes differentiation with respect to r.

3 Stress distributions

The Navier equation for the radial displacement u_r was given in Eq. (5). It is a non-homogenous form of Euler–Cauchy equation. Solutions of Eq. (5) for two cases of temperature distribution are given below.

3.1 Temperature distribution with considering $\beta_3 \neq -1$

In the steady-state condition, the heat conduction equation for the one-dimensional problem in spherical coordinate system simplifies to

$$\frac{1}{r^2}\frac{d}{\mathrm{d}r}\left(r^2\lambda(r)\frac{\mathrm{d}T(r)}{\mathrm{d}r}\right) = 0, \tag{7}$$

The thermal boundary condition for an FGM hollow sphere is given as

$$\lambda(r)\frac{\mathrm{d}T}{\mathrm{d}r} = h_i(T - T_i), \quad \text{on } r = 1 \tag{8a}$$

$$-\lambda(r)\frac{\mathrm{d}T}{\mathrm{d}r} = h_o(T - T_o), \quad \text{on } r = k \tag{8b}$$

where T_i and T_o are the temperatures of the surrounding media, h_i and h_o are the transfer coefficient, and subscripts i and o correspond to surfaces $R = a$ and $R = b$, respectively.

Using relation (1c), and the boundary conditions (8), the general solution of Eq. (7) becomes

$$T(r) = c_5 r^{-(\beta_3+1)} + c_6, \tag{9}$$

where

$$c_5 = \frac{(T_i - T_o)}{\lambda_i(\beta_3+1)[\frac{1}{k^2 h_o} + \frac{1}{h_i}] - (\frac{1}{k^{\beta_3+1}} - 1)}, \tag{10a}$$

$$c_6 = \frac{\lambda_i(\beta_3+1)[\frac{T_i}{k^2 h_o} + \frac{T_o}{h_i}] - (\frac{T_i}{k^{\beta_3+1}} - T_o)}{\lambda_i(\beta_3+1)[\frac{1}{k^2 h_o} + \frac{1}{h_i}] - (\frac{1}{k^{\beta_3+1}} - 1)}. \tag{10b}$$

By substituting Eqs. (10) and (9) into Eq. (5), the Navier equation would be

$$r^2 u_r'' + A r u_r' + B u_r = C r^{\beta_2-\beta_3} + D r^{\beta_2+1}, \tag{11}$$

where

$$C = \alpha_i \frac{1+\nu}{1-\nu}(\beta_1 + \beta_2 - \beta_3 - 1)c_5, \tag{12a}$$

$$D = \alpha_i \frac{1+\nu}{1-\nu}(\beta_1 + \beta_2)c_6. \tag{12b}$$

Equation (11) is the non-homogeneous Euler differential equation with general and particular solutions whose complete solution u_r is

$$u(r) = c_1 r^{m_1} + c_2 r^{m_2} + c_3 r^{\beta_2 - \beta_3} + c_4 r^{\beta_2 + 1}, \tag{13}$$

where $m_{1,2}$ are given by homogeneous solution as following

$$m_{1,2} = \frac{1 - A \pm \sqrt{\Delta}}{2}, \quad \Delta = (A-1)^2 - 4B, \tag{14a, b}$$

c_3 and c_4 can be calculated by substituting particular solutions into Eq. (11) as

$$c_3 = \frac{C}{(\beta_2 - \beta_3 - 1 + A)(\beta_2 - \beta_3) + B}, \tag{15a}$$

$$c_4 = \frac{D}{(\beta_2 + A)(\beta_2 + 1) + B}. \tag{15b}$$

By substituting Eq. (11) into Eqs. (3a, b) and (4), the resulting stress expressions are

$$\sigma_r = \frac{E_i r^{\beta_1}}{(1+\nu)(1-2\nu)} \left\{ c_1 Q_1 r^{m_1 - 1} + c_2 Q_2 r^{m_2 - 1} + c_3 Q_3 r^{\beta_2 - \beta_3 - 1} + c_4 Q_4 r^{\beta_2} - (1+\nu)\alpha_i r^{\beta_2} T(r) \right\}, \tag{16a}$$

$$\sigma_\phi = \frac{E_i r^{\beta_1}}{(1+\nu)(1-2\nu)} \left\{ c_1 G_1 r^{m_1 - 1} + c_2 G_2 r^{m_2 - 1} + c_3 G_3 r^{\beta_2 - \beta_3 - 1} + c_4 G_4 r^{\beta_2} - (1+\nu)\alpha_i r^{\beta_2} T(r) \right\}, \tag{16b}$$

where

$$Q_1 = 2\nu + (1-\nu)\, m_1, \qquad G_1 = 1 + \nu m_1, \tag{17a}$$

$$Q_2 = 2\nu + (1-\nu)\, m_2, \qquad G_2 = 1 + \nu m_2, \tag{17b}$$

$$Q_3 = (\beta_2 - \beta_3)(1-\nu) + 2\nu, \qquad G_3 = (\beta_2 - \beta_3)\nu + 1, \tag{17c}$$

$$Q_4 = (\beta_2 + 1)(1-\nu) + 2\nu, \qquad G_4 = (\beta_2 + 1)\nu + 1. \tag{17d}$$

In Eq. (16), c_1 and c_2 are unknown constants that can be obtained by applying boundary condition. For the hollow sphere submitted to uniform pressures p_i and p_o on the inner and outer surfaces, respectively, the mechanical boundary conditions can be expressed as

$$\sigma_r \Big|_{r=1} = -p_i, \quad \text{on } r = 1, \tag{18a}$$

$$\sigma_r \Big|_{r=k} = -p_o\,, \quad \text{on } r = k. \tag{18b}$$

Note that these are normalized form of what were mentioned in [14].

Substituting the boundary conditions (18) into Eq. (16), the constants of integration become

$$c_1 = \frac{1}{Q_1 (k^{m_1} - k^{m_2})} \left\{ c_3 Q_3 (k^{m_2} - k^{\beta_2 - \beta_3}) + c_4 Q_4 (k^{m_2} - k^{1+\beta_2}) - (1+\nu)\alpha_i (k^{m_2} T_i - k^{1+\beta_2} T_o) \right\} + \frac{(1+\nu)(1-2\nu)}{E_i Q_1 (k^{m_1} - k^{m_2})} \left\{ k^{m_2} p_i - k^{1-\beta_1} p_o \right\}, \tag{19a}$$

$$c_2 = -\frac{1}{Q_2 (k^{m_1} - k^{m_2})} \left\{ c_3 Q_3 (k^{m_1} - k^{\beta_2 - \beta_3}) + c_4 Q_4 (k^{m_1} - k^{\beta_2 + 1}) - (1+\nu)\alpha_i (k^{m_1} T_i - k^{1+\beta_2} T_o) \right\} - \frac{(1+\nu)(1-2\nu)}{E_i Q_2 (k^{m_1} - k^{m_2})} \left\{ k^{m_1} p_i - k^{1-\beta_1} p_o \right\}. \tag{19b}$$

3.2 Temperature distribution with considering $\beta_3 = -1$

In the steady-state condition, the heat conduction equation for the one-dimensional problem in spherical coordinate system with considering $\beta_3 = -1$ simplifies to

$$\frac{1}{r^2}\frac{d}{\mathrm{d}r}\left(\lambda_i r \frac{\mathrm{d}T(r)}{\mathrm{d}r}\right) = 0, \tag{20}$$

The thermal boundary condition for an FGM hollow sphere is given as:

$$\frac{\lambda_i}{r}\frac{\mathrm{d}T}{\mathrm{d}r} = h_i(T - T_i), \quad \text{on } r = 1, \tag{21a}$$

$$-\frac{\lambda_i}{r}\frac{\mathrm{d}T}{\mathrm{d}r} = h_o(T - T_o), \quad \text{on } r = k. \tag{21b}$$

The general solution of Eq. (20) with considering relation of thermal conductivity coefficient (1c) and boundary conditions (21) is

$$T(r) = c_5 \ln r + c_6, \tag{22}$$

where

$$c_5 = -\frac{(T_i - T_o)}{(\ln k + \frac{\lambda_i}{h_o k^2}) + \frac{\lambda_i}{h_i}}, \tag{23a}$$

$$c_6 = \frac{(\ln k + \frac{\lambda_i}{h_o k^2})T_i + \frac{\lambda_i T_o}{h_i}}{(\ln k + \frac{\lambda_i}{h_o k^2}) + \frac{\lambda_i}{h_i}}. \tag{23b}$$

By substituting Eq. (22) into Eq. (5) yields

$$r^2 u_r'' + A r u_r' + B u_r = C r^{\beta_2+1} \ln r + D r^{\beta_2+1}, \tag{24}$$

where

$$C = \alpha_i \frac{1+\nu}{1-\nu}(\beta_1 + \beta_2)c_6, \tag{25a}$$

$$D = \alpha_i \frac{1+\nu}{1-\nu}\{(\beta_1 + \beta_2)c_6 + c_5\}. \tag{25b}$$

Equation (24) is the non-homogeneous Euler differential equation with general and particular solutions. Considering the solutions of homogeneous form of this equation which was presented in previous section, we know that general solution of homogenous form of above Euler–Cauchy equation is

$$u_h(r) = c_1 r^{m_1} + c_2 r^{m_2}, \tag{26}$$

where $m_{1,2}$ are presented in Eq. (14a, b).

The particular solution $u_p(r)$is assumed to have the form

$$u_p(r) = c_3 r^{\beta_2+1} \ln r + c_4 r^{\beta_2+1}, \tag{27}$$

where c_3 and c_4 can be determined by substituting particular solutions in Eq. (24) as following

$$c_3 = \frac{C}{(\beta_2 + A)(\beta_2 + 1) + B}, \tag{28a}$$

$$c_4 = \frac{D}{(\beta_2 + A)(\beta_2 + 1) + B}. \tag{28b}$$

The complete solution for $u(r)$ is the sum of general and particular solutions as

$$u(r) = u_g(r) + u_p(r), \tag{29}$$

Thus,

$$u(r) = c_1 r^{m_1} + c_2 r^{m_2} + c_3 r^{\beta_2+1} \ln r + c_4 r^{\beta_2+1}. \tag{30}$$

By substituting Eq. (30) into Eqs. (3a, b) and (4), the resulting stress expressions are

$$\sigma_r = \frac{E_i r^{\beta_1}}{(1+\nu)(1-2\nu)} \left\{ c_1 Q_1 r^{m_1-1} + c_2 Q_2 r^{m_2-1} + c_3 Q_3 r^{\beta_2} \ln r + c_4 Q_4 r^{\beta_2} - (1+\nu)\alpha_i r^{\beta_2} T(r) \right\}, \tag{31a}$$

$$\sigma_\phi = \frac{E_i r^{\beta_1}}{(1+\nu)(1-2\nu)} \left\{ c_1 G_1 r^{m_1-1} + c_2 G_2 r^{m_2-1} + c_3 G_3 r^{\beta_2} \ln r + c_4 G_4 r^{\beta_2} - (1+\nu)\alpha_i r^{\beta_2} T(r) \right\}, \tag{31b}$$

where

$$Q_1 = 2\nu + (1-\nu)\, m_1, \qquad G_1 = 1 + \nu m_1, \tag{32a}$$

$$Q_2 = 2\nu + (1-\nu)\, m_2, \qquad G_2 = 1 + \nu m_2, \tag{32b}$$

$$Q_3 = (\beta_2 + 1)(1-\nu) + 2\nu, \qquad G_3 = (\beta_2+1)\nu + 1, \tag{32c}$$

$$Q_4 = \left(\frac{C}{D} + \beta_2 + 1\right)(1-\nu) + 2\nu, \quad G_4 = \left(\frac{C}{D} + \beta_2 + 1\right)\nu + 1. \tag{32d}$$

and the constants c_1 and c_2 are determined from the boundary conditions (18) as

$$c_1 = \frac{1}{Q_1 (k^{m_1} - k^{m_2})} \left\{ -c_3 Q_3 k^{\beta_2+1} \ln k + c_4 Q_4 (k^{m_2} - k^{1+\beta_2}) - (1+\nu)\alpha_i (k^{m_2} T_i - k^{1+\beta_2} T_o) \right\}$$
$$+ \frac{(1+\nu)(1-2\nu)}{E_i Q_1 (k^{m_1} - k^{m_2})} \left\{ k^{m_2} p_i - k^{1-\beta_1} p_o \right\}, \tag{33a}$$

$$c_2 = -\frac{1}{Q_2 (k^{m_1} - k^{m_2})} \left\{ -c_3 Q_3 k^{\beta_2+1} \ln k + c_4 Q_4 (k^{m_1} - k^{\beta_2+1}) - (1+\nu)\alpha_i (k^{m_1} T_i - k^{1+\beta_2} T_o) \right\}$$
$$- \frac{(1+\nu)(1-2\nu)}{E_i Q_2 (k^{m_1} - k^{m_2})} \left\{ k^{m_1} p_i - k^{1-\beta_1} p_o \right\}. \tag{33b}$$

4 Finite element analysis

A geometry specimen was modeled using a commercial FE code, ABAQUS, for a comparative study. In the FEM model, due to symmetry, only a quarter of the sphere specimen geometry was considered. An 8-node axisymmetric quadrilateral element was used to represent the FGM specimen. The final FEM model consisted of 1580 elements in total. In the model, the variation in material properties was implemented by having 20 layers, with each layer having a constant value of material properties. Figure 2 illustrates the meshing region.

The nodal points along the horizontal edge passing through the center were free to move in X direction but were constrained from moving in the Y direction to reflect the symmetry of sphere specimen geometry.

5 Result and discussion

The analytical solution and numerical analysis presented in the previous section were applied to a thick hollow sphere of inner radius, $a = 40$ mm, and outer radius of $b = 60$ mm.

A special case is considered in which there is no heat transfer taking place between the inner and outer surfaces with the surrounding medium ($h_i, h_o \to \infty$) and the surface temperature at the inner and outer surfaces is prescribed as T_i and T_o, respectively. The boundary conditions for temperature are taken as $T_i = 300°\text{C}$, $T_o = 25°\text{C}$. The modulus of elasticity and the thermal coefficient of expansion at the inner surface of the sphere were taken as $E_i = 200$ GPa and $\alpha_i = 1.2(10^{-6})/°\text{C}$, respectively. It is also assumed that the Poisson's ratio ν has a constant value of 0.3. The power index for the modulus of elasticity, coefficient of thermal expansion, and heat conduction coefficient are assumed to be identical ($\beta_1 = \beta_2 = \beta_3 = \beta$).

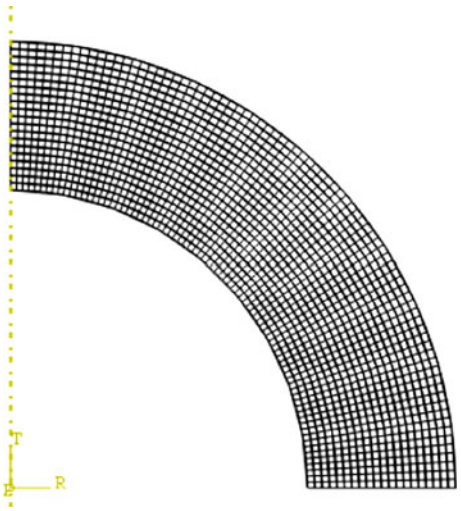

Fig. 2 Finite element mesh region

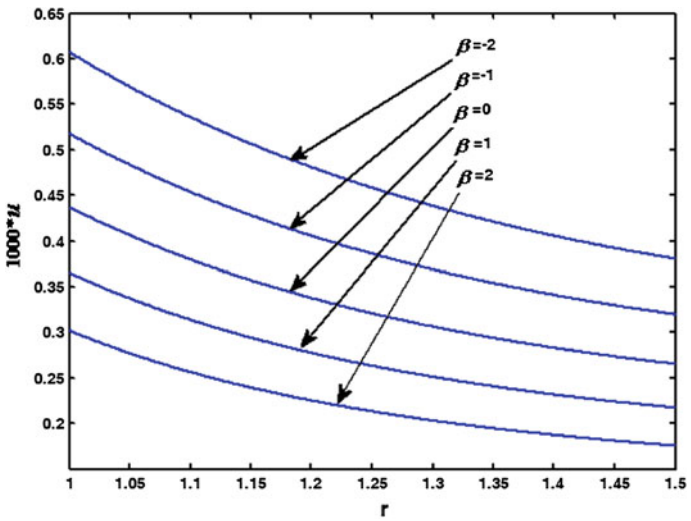

Fig. 3 Distribution of normalized radial displacement under the loading of pressure

5.1 Pressure only

Consider the thick sphere is subjected to mechanical stresses. The inside pressure is assumed to be $p = 80\,MPa$, and outside pressure, zero. For different values of β, radial displacement, radial stress, and circumferential stress along the radial direction are plotted in Figs. 3, 4, and 5. The results for radial stress and circumferential stress were normalized with respect to internal pressure loading. (Note that $u(r) = \frac{U(R)}{a}$ are normalized form of what were mentioned in [14])

Here, a higher value of β means increasing stiffness (see Eq. 1a, b, c). It is observed that the radial stress and the radial displacement increase as the power law index of FGM sphere decreases.

The mechanical circumferential stress versus the radial direction is shown in Fig. 5. It is seen that for $\beta < 1$ the circumferential stress variations decrease along the radial direction. When $\beta > 1$, the situation is reversed and the circumferential stress increases along the radial direction. The curve associated with $\beta = 1$ shows that the variation in circumferential stress along the radial direction is minor and is almost uniform across the radius. At an approximate radial distance of $r = 1.23$, the stress values for all values of β converge toward the stress values in the homogenous material ($\beta = 0$).

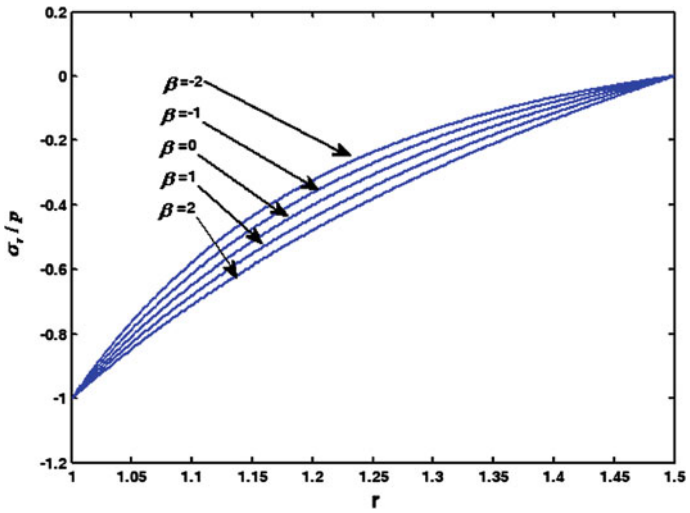

Fig. 4 Distribution of normalized radial stress under the loading of pressure

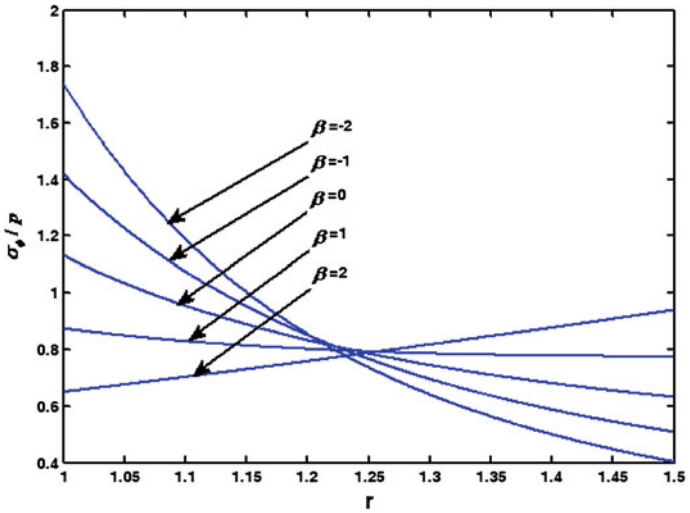

Fig. 5 Distribution of normalized circumferential stress under the loading of pressure

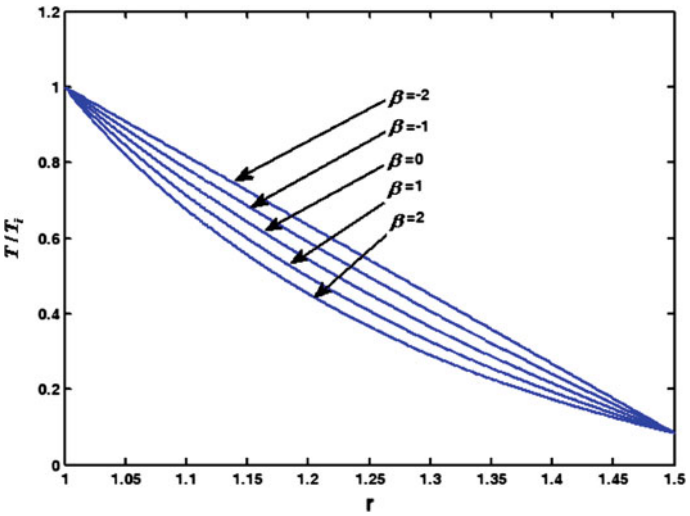

Fig. 6 Distribution of normalized radial temperature under the loading of temperature

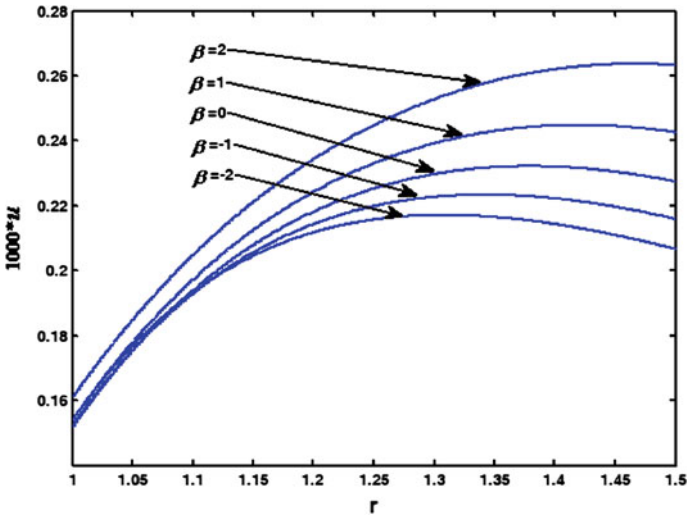

Fig. 7 Distribution of normalized radial displacement under the loading of temperature

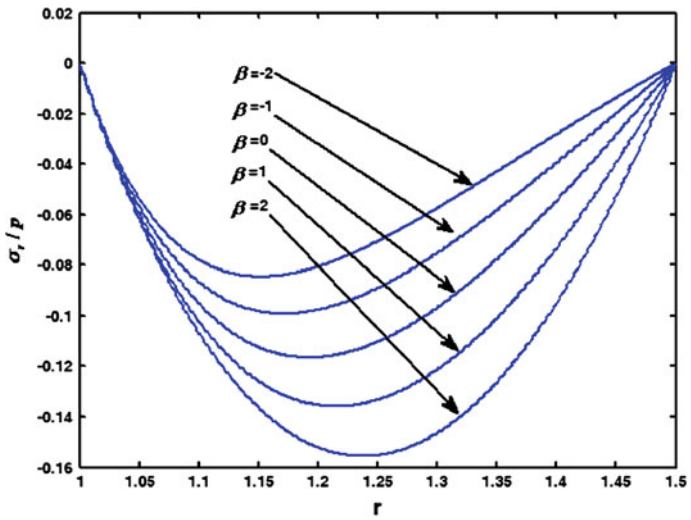

Fig. 8 Distribution of normalized radial stress under the loading of temperature

5.2 Temperature only

Now the hollow sphere assumed to be traction free at inner and outer surfaces. Temperature profile, radial displacement, radial stress, and circumferential stress along the radial direction are plotted in Figs. 6, 7, 8, and 9. Figure 6 shows the temperature distribution across the wall thickness. This figure shows that as β increases, the temperature decreases. Figure 7 shows the resulting thermoelastic radial displacement due to the given temperature variations. It is seen that for higher β values, the radial displacement increases. This increase is greater for outer layers. Figure 8 represents the radial stress along the radial direction satisfying the traction free boundary conditions. Also, this figure shows that as the power law index increases, the compressive stresses in the middle layers increase. The circumferential stress versus radial direction is shown in Fig. 9. It is observed that the circumferential stress distributions are compressive at the inside surface and tensile at the outside surface. It is observed that at approximate radial distances of $r = 1.01$ and $r = 1.32$, the stress values for all values of β converge toward the stress values in the homogenous material ($\beta = 0$). From the figures, it can be seen that the temperature loading has a greater effect on radial displacement and circumferential stress in comparison with radial stress.

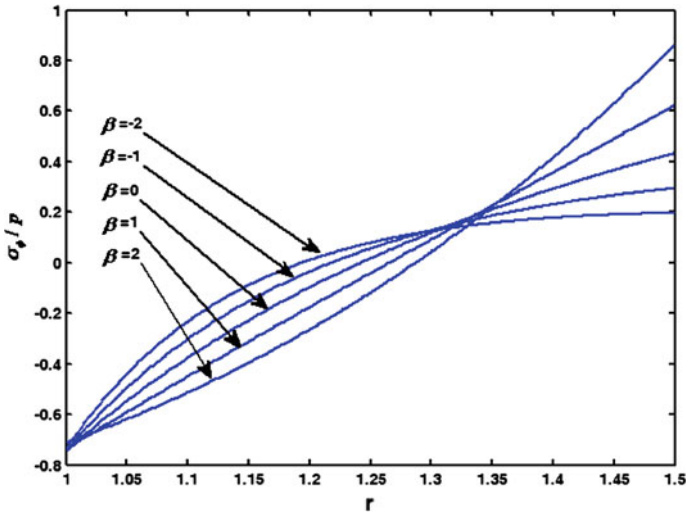

Fig. 9 Distribution of normalized circumferential stress under the loading of temperature

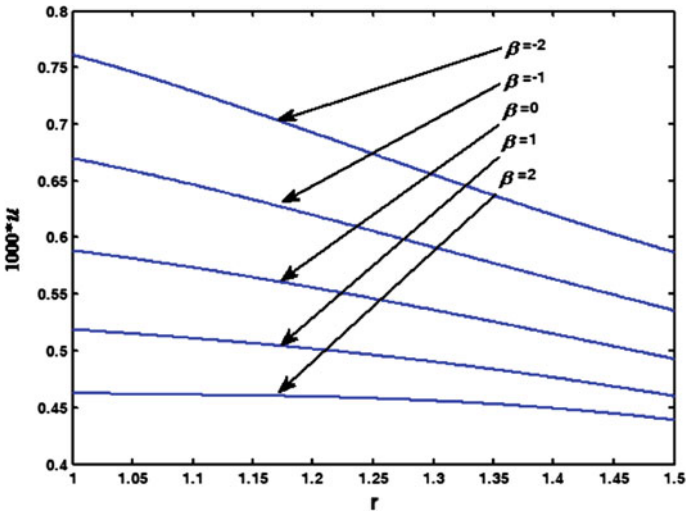

Fig. 10 Distribution of normalized radial displacement under the combined loading of pressure and temperature

5.3 Combined loading (pressure + temperature)

Since both pressure and temperature loadings are in the elastic range, the principle of superposition was applied for the combined loading and the following results were obtained. For different values of β, radial displacement, radial stress, and circumferential stress along the radial direction are shown in Figs. 10, 11, and 12. Because of the opposite effect of mechanical loading (pressure in inner surface) on radial displacement and circumferential stress in comparison with thermo-mechanical loading, it can be observed from Figs. 10 and 12 that the rate of increase or decrease in the results decreases due to the effect of combined temperature and pressure loading. Thus, as shown in Fig. 10, the rate of radial displacement variation is minimum for $\beta = -2$. Also, Figs. 10 and 12 show that as the power law index increases, the rate of radial displacement and circumferential stress variation decrease, whereas the situation is reversed for radial stress as shown in Fig. 11.

5.4 Validate FEM

The results obtained in FEM study were compared with previously described analytical results. Tables 1 and 2 show the results for $\beta = -1$ and $\beta = 1$, respectively, for the case of combined loading. It can be seen in the

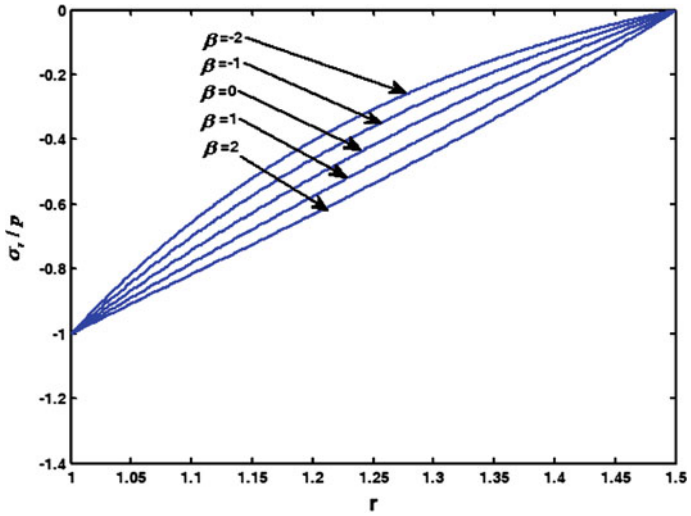

Fig. 11 Distribution of normalized radial stress under the combined loading of pressure and temperature

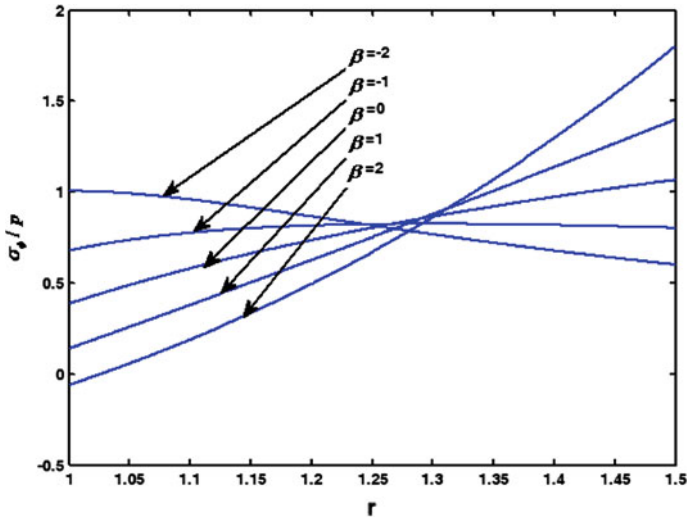

Fig. 12 Distribution of normalized circumferential stress under the combined loading of pressure and temperature

Table 1 Comparison of numerical data from analytical (Eqs. 22, 29 and 30) and FEM calculations along the radial normalized direction for the power law index ($\beta = -1$)

r	Type	$\frac{T}{T_i}$		$u_r * 1{,}000$		$\frac{\sigma_r}{p}$		$\frac{\sigma_\phi}{p}$	
		Value	%Err	Value	%Err	Value	%Err	Value	%Err
1	Anal.	1.00000	0	0.66977	0.00572	−1.00000	0.03888	0.67776	0.28864
	FEM	1.00000		0.66981		−0.99961		0.67972	
1.0875	Anal.	0.81036	0.01902	0.64972	0.00311	−0.73310	0.02460	0.76688	0.02103
	FEM	0.81052		0.64970		−0.73328		0.76672	
1.1875	Anal.	0.61148	0.02158	0.62312	0.00099	−0.48683	0.03391	0.81198	0.01272
	FEM	0.61162		0.62311		−0.48699		0.81187	
1.2875	Anal.	0.42870	0.02658	0.59488	0.00024	−0.29169	0.04892	0.82416	0.00791
	FEM	0.42881		0.59489		−0.29184		0.82410	
1.3875	Anal.	0.25959	0.03682	0.56649	0.00114	−0.13687	0.08734	0.81890	0.00549
	FEM	0.25968		0.56650		−0.13699		0.81885	
1.5	Anal.	0.08333	0	0.53548	0.00241	0.00000	–	0.80236	0.78734
	FEM	0.08333		0.53550		0.00009		0.80867	

Table 2 Comparison of numerical data from analytical (Eqs. 9, 16 and 13) and FEM calculations along the radial normalized direction for the power law index ($\beta = 1$)

r	Type	$\frac{T}{T_i}$		$u_r * 1{,}000$		$\frac{\sigma_r}{p}$		$\frac{\sigma_\phi}{p}$	
		Value	%Err	Value	%Err	Value	%Err	Value	%Err
1	Anal.	1	0	0.51872	0.02139	−1	0.00300	0.13829	1.1281
	FEM	1		0.51883		−0.99997		0.13673	
1.0875	Anal.	0.74516	0.07679	0.51197	0.03757	−0.80773	0.01459	0.34923	0.06286
	FEM	0.74574		0.51216		−0.80785		0.34901	
1.1875	Anal.	0.52008	0.07952	0.50288	0.03858	−0.60100	0.01497	0.59547	0.01202
	FEM	0.52050		0.50307		−0.60109		0.59540	
1.2875	Anal.	0.34538	0.08746	0.49172	0.03975	−0.40338	0.01273	0.84718	0.00693
	FEM	0.34568		0.49192		−0.40343		0.84724	
1.3875	Anal.	0.20707	0.10594	0.47815	0.04110	−0.21159	0.00287	1.10446	0.01601
	FEM	0.20729		0.47835		−0.21159		1.10464	
1.5	Anal.	0.08333	0	0.45973	0.04140	0	–	1.40083	0.64545
	FEM	0.08333		0.45992		0.00006		1.39179	

Tables that the % errors are rather small and, in almost all cases, are less than 0.1% except for inner surface and outer surface in circumferential stress in which the differences increase up to 1.12%. The assumption of constant modulus of elasticity in each layer leads to this increase of error.

6 Conclusion

This paper presents an analytical and numerical solution to obtain the spherically symmetric thermal and mechanical stresses in a thick hollow sphere made of functionally graded material under the combined pressure and temperature loading. The material properties are assumed to be graded along the radial direction according to a power law function. It is observed by defining the normalized parameter $r = \frac{R}{a}$, solution process, and applying the boundary conditions could be easier. Also, this method would lead to simpler analytical formulations.

In this paper, heat conduction and Navier equations were solved for $\beta_3 = -1$ and other values of β_3 separately. Comparison between the results from the analytical findings and the numerical simulations indicates that the errors are less than 0.1% for FGM specimens.

From above results, it can be concluded that the power law index has a great effect on stresses and radial displacement distributions in FGM sphere. Thus, the power law index of FGM sphere is a useful parameter from a design point of view and can be tailored to specific applications to control the stress distributions. Finally, we can find an optimum value for β such that variation in stresses along the radial direction is minimized.

References

1. Yamanouchi, M., Koizumi, M., Shiota, I.: Proceedings of the First International Symposium on Functionally Gradient Materials, Japan, pp. 273–281 (1990)
2. Koizumu, M.: The concept of FGM, ceramic transactions. Funct. Grad. Mater. **34**, 3–10 (1993)
3. Tanigawa, Y.: Some basic thermoelastic problems for nonhomogeneous structural materials. Appl. Mech. Rev. **48**, 89–377 (1995)
4. Obata, Y., Noda, N.: Steady thermal stresses in a hollow circular cylinder and a hollow sphere of a functionally gradient material. J. Therm. Stress **17**, 88–471 (1994)
5. Kim, K.S., Noda, N.: Green's function approach to unsteady thermal stresses in an infinite hollow cylinder of functionally graded material. Acta. Mech. **156**, 61–145 (2002)
6. Horgan, C.O., Chan, A.M.: The pressurized hollow cylinder or disk problem for functionally graded isotropic linearly elastic materials. J. Elast. **55**, 43–59 (1999)
7. Nayebi, A., El Abdi, R.: Cyclic plastic and creep behaviour of pressure vessels under thermomechanical loading. Comput. Mater. Sci. **25**, 96–285 (2002)
8. Praveen, G.N., Reddy, J.N.: Nonlinear transient thermoelastic analysis of functionally graded ceramic–metal plates. Int. J. Solids Struct. **35**, 76–4457 (1998)
9. Reddy, J.N., Chin, C.D.: Thermomechanical analysis of functionally graded cylinders and plates. Int. J. Solids Struct. **21**, 593–626 (1998)
10. Praveen, G.N., Chin, C.D., Reddy, J.N.: Thermoelastic analysis of a functionally graded ceramic–metal cylinder. ASCE J. Eng. Mech. **125**, 67–1259 (1999)

11. Reddy, J.N.: Analysis of functionally graded plates. Int. J. Numer. Meth. Eng. **47**, 84–663 (2000)
12. Reddy, J.N., Cheng, Z.Q.: Three-dimensional thermomechanical deformations of functionally graded rectangular plates. Eur. J. Mech. A Solid **20**, 60–841 (2001)
13. Reddy, J.N., Cheng, Z.Q.: Frequency of functionally graded plates with three-dimensional asymptotic approach. J. Eng. Mech. **129**, 896–900 (2003)
14. Johnson, W., Mellor, P.B.: Engineering Plasticity: Ellis Harwood Ltd, Chichester (1983)
15. Zimmerman, R.W., Lutz, M.P.: Thermal stresses and thermal expansion in a uniformly heated functionally graded cylinder. J. Therm. Stress **22**, 177–188 (1999)
16. Tutuncu, N., Ozturk, M.: Exact solutions for stresses in functionally graded pressure vessels. Compos. Part B Eng. **32**, 683–686 (2001)
17. Jabbari, M., Sohrabpour, S., Eslami, M.R.: Mechanical and thermal stresses in a functionally graded hollow cylinder due to radially symmetric loads. Int. J. Press. Vessel. Pipi. **79**, 493–497 (2002)
18. Eslami, M.R., Babaei, M.H., Poultangari, R.: Thermal and mechanical stresses in a fg thick sphere. Int. J. Press. Vessel. Pip. **82**, 522–527 (2005)
19. Poultangari, R., Jabbari, M., Eslami, M.R.: Functionally graded hollow spheres under non-axisymmetric thermo-mechanical loads. Int. J. Press. Vessel. Pip. **85**, 295–305 (2008)
20. You, L.H., Zhang, J.J., You, X.Y.: Elastic analysis of internally pressurized thick-walled spherical pressure vessels of functionally graded materials. Int. J. Press. Vessel. Pip. **82**, 347–354 (2004)
21. Pan, E., Roy, A.K.: A simple plane-strain solution for functionally graded multilayered isotropic cylinders. Struct. Eng. Mech. **24**, 727–740 (2006)
22. Jabbari, M., Mohazza, A.H., Bahtui, A., Eslami, M.R.: Analytical solution for three-dimensional stresses in a short length FGM hollow cylinder. ZAMM. Z. Angew. Math. Mech. **87**, 413–429 (2007)
23. You, L.H., Ou, H., Li, J.: Stress analysis of functionally graded thickwalled cylindrical vessels. AIAA J. **45**, 2790–2798 (2007)
24. Bahtui, A., Poultangari, R., Esalami, M.R.: Thermal and Mechanical Stresses in Thick Spheres with an Extended FGM Model. Brunel University Research Archive, School of Engineering and Design Research Papers (2008)
25. Tutuncu, N.: Stresses in thick-walled FGM cylinders with exponentially-varying properties. Eng. Struct. **29**, 2032–2035 (2007)
26. Chen, Y.Z., Lin, X.Y.: Elastic analysis for thick cylinders and spherical pressure vessels made of functionally graded materials. Comput. Mater. Sci. **44**, 58–587 (2008)
27. Zamani Nejad, M., Rahimi, G.H.: Deformations and stresses in rotating FGM pressurized thick hollow cylinder under thermal load. Sci. Res. Essay **4**(3), 131–140 (2009)
28. Abrinia, K., Naee, H., Sadeghi, F., Djavanroodi, F.: New analysis for the FGM thick cylinders under combined pressure and temperature loading. Am. J. Appl. Sci. **5**(7), 852–859 (2008)
29. Tutuncu, N., Temel, B.: A novel approach to stress analysis of pressurized FGM cylinders, disks and spheres. Compos. Struct. **91**, 385–390 (2009)